1-1-2012

A validated thermal model of bead-on-plate welding

Djarot Darmadi
University of Wollongong, dbd991@uow.edu.au

A K. Tieu
University of Wollongong, ktieu@uow.edu.au

John Norrish
University of Wollongong, johnn@uow.edu.au

Heat Mass Transfer (2012) 48:1219–1230
DOI 10.1007/s00231-012-0970-5

ORIGINAL

A validated thermal model of bead-on-plate welding

Djarot B. Darmadi · Anh Kiet Tieu · John Norrish

Received: 31 July 2011 / Accepted: 3 January 2012 / Published online: 15 January 2012

Abstract In this paper, finite element model is used to carry out thermal analysis of bead-on-plate welding. The model followed the proposed five step strategies which were then built into a model to obtain temperature history at the positions of thermocouples. Temperature field was also evaluated by comparing predicted weld bead with the actual weld bead. Using these proposed strategies, well matched temperature histories and temperature field have been obtained.

List of symbols

α	Diffusivity (m^2/s)
ρ	Density (kg/m^3)
ξ	Moving coordinate abscissa parallel to z axis
c	Specific heat (J/kg K)
e_{rad}	Emissivity
E	Young's modulus (N/m^2)
h_{conv}	Convection heat transfer coefficient ($watt/m^2$ K)
$I_0(p)$	Modified Bessel function first kind, order zero
k	Thermal conductivity (watt/m K)
$\dot{q}$	Heat rate (J/s)
$\dot{q}''$	Heat flux rate (J/s m^2)
$\dot{q}'''$	Heat rate generated at a body (J/s m^3)
r_e	Equivalent heat source geometric parameter model (m or mm)
r_x, r_y, r_z	Heat source geometric parameters model (m or mm)
S	Weld line length (mm)
t, τ	Time, time increment (s)
T, T_o	Temperature, initial temperature (°C)
v	Welding speed (m/s or mm/s)

D. B. Darmadi (✉)
School of Mechanical Engineering, Brawijaya University, Malang, Indonesia
e-mail: b_darmadi_djarot@yahoo.co.id

A. K. Tieu · J. Norrish
School of Mechanical Engineering, University of Wollongong, Wollongong, Australia

1 Introduction

Welding applications subject materials to non-uniform temperature cycles. This non-uniformity causes problems which in turn lead to premature fatigue damage, stress corrosion and fracture [1–4]. Studies of transient temperature distributions in weldments are important for weld quality control and as an aid to welding procedure development [5].

Rosenthal [6] proposed an analytic solution for a point moving heat source that can be applied to the welding process. Following this, the analytic solutions for moving heat sources attracted much attention, [7–10]. More recently the high speed computational resources needed for numerical analysis have become more readily available and FEM has become a popular tool for weld modeling. An advantage of numerical analysis over the analytic method is the ability to obtain a solution for complex geometry and boundary conditions which may be difficult to achieve using analytic solutions.

A major issue in modeling is accuracy and validity. To this end the European Network on Neutron Techniques Standardization for Structural Integrity (NeT) has published experimental data and procedures which can be accessed at https://odin.jrc.ec.europa.eu [11, 12]. Experimental work was carried out using bead-on-plate (bop) welding. Nine thermocouples are attached at different measured points.

A welding model is built based on assumptions. An assumed condition in the model may be able to fit the temperature history of one thermocouple but it would affect adversely to others. Overall it can be said that the bead-on-plate welding is a challenging benchmark. Based on the published data researchers have aimed to develop standards finite element models of welding. The data obtained from NeT [12] were used to validate the accuracy of the FEM model.

This paper presents a comprehensive FEM model using a five steps strategy to provide unknown values or modes which are inputs for the model. Those values are welding efficiency, heat source parameters, dwell-time at the start and end of the arc, arc extinguishing mode, convection heat transfer coefficient and radiation emissivity. Those values from previous literature vary widely depending on the assumptions made and it is not surprising that resultant temperature histories differ. Using the proposed strategies, a bead-on-plate welding thermal model has been established based on a systematic procedure and realistic conditions that can predict accurately the transient thermal history of the weld.

2 Welding procedure

A complete welding procedure can be obtained at https://odin.jrc.ec.europa.eu [12]. The welding procedures are summarized in Table 1. Four identical plate specimens (called as A11, A12, A21 and A22) are produced. A sketch diagram for the welding set up and thermocouple positions are presented in Figs. 1 and 2 respectively. It should be noted that the origin of coordinate system is at the weld stop end. The positions of the thermocouples based on the chosen coordinate system are tabulated in Table 2.

Table 1 Summary of welding procedure

Parent material
Size: 120 × 180 × 17 mm
AISI Type 316L austenitic stainless steels
Residual stress is relieved using heat treatment
Filler
∅0.8 mm
Type: 316S96
Spec: A5.9.93 (ASME); ER316H
Welding parameters
Welding process: tungsten inert gas (TIG)
Type: bead-on-plate
Weld length: 60 mm
Heat input: 633 J/mm
Welding speed: 2.27 mm/s

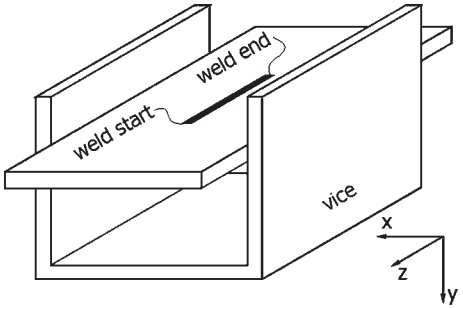

Fig. 1 Sketch of welding process and coordinate system

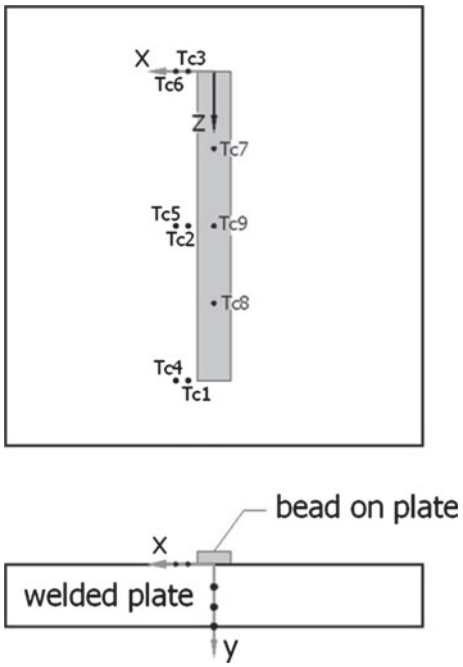

Fig. 2 Thermocouple position on weld on bead welded plate

Four sets of temperature histories for four specimens were obtained from nine thermocouples. As the thermocouple Tc8 was not pushed far enough into the hole and there is no clear reference to where the data was obtained, the Tc8 thermocouple was not considered. For thermocouple Tc9, the data from specimen A21 were also excluded since they showed a lower temperature and inconsistent with data from other specimens [13].

The temperature dependent properties of the base metal and welding filler were obtained from NeT [12]. The material properties for the base metal and the weld metal are shown at Table 3. The density and Poisson's ratio for both materials are 7,966 kg/m^3 and 0.294 respectively. In Fig. 3 are shown thermal properties for both metals graphically.

The temperature dependent properties of the base metal and welding filler were obtained from NeT [12]. The

Table 2 Thermocouple mean-position [12]

Thermocouple	Mean position (mm)		
	X	*Y*	*Z*
T1	8.50	1.24	60
T2	8.00	1.20	30
T3	7.50	1.24	0
T4	11.50	1.21	60
T5	11.50	1.23	30
T6	12.00	1.18	0
T7	0	10.50	15
T8	0	4.67	46
T9	0	17.00	30

material properties for the base metal and the weld metal are shown at Table 3. The density and Poisson's ratio for both materials are 7,966 kg/m^3 and 0.294 respectively. In Fig. 3 are shown thermal properties for both metals graphically.

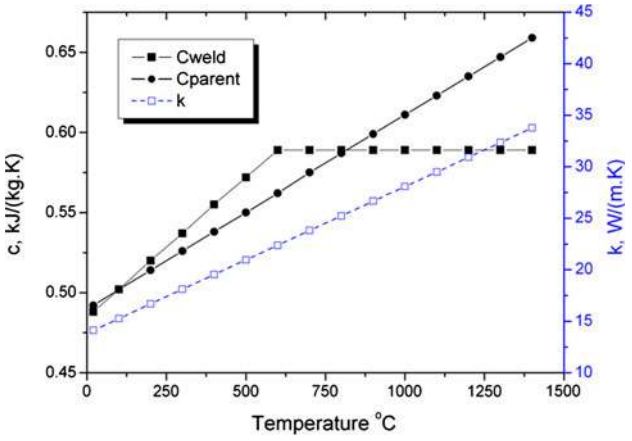

Fig. 3 Temperature dependence of thermal properties [12]

3 Previous work in weld modeling of the net welding procedure

There are two main techniques used in weld modeling, the standard technique and the birth-and-death technique. Basically in the standard technique the weld bead is modeled in situ whilst the element birth-and-death technique considers growing weld bead. Further detail can be found in Sects. 4.2 and 4.3.

Based on the data provided by NeT, there are at least eight participants involved in weld modeling. British Energy-Frazer-Nash Consultancy, UK [14] modeled the welding process using ABAQUS. The moving heat source is modeled as Goldak's ellipsoidal distributed heat source. Two different sets of parameters for the heat source were used: $r_x = 2.8$ mm, $r_y = 2.8$ mm, $r_z = 0.7$ mm and $r_x = 1.6$ mm, $r_y = 1.6$ mm, $r_z = 0.4$ mm with the heat efficiency set to 75 and 60% respectively. At the weld start point different dwell times were used for each model, 1.5 s dwell is used for the first model and 0.7 s dwell is used for the second model. Convection was represented by $h_{\text{conv}} = 4.2$ W/m^{2}K at 100°C and $h_{\text{conv}} = 11.8$ W/m^{2}K at 1,000°C. Radiation was modeled using an emissivity of 0.4. For both models the element birth and death technique was used.

Imperial College, UK also used the ABAQUS code for the welding simulation [15]. The standard and the element birth and death techniques were used with a moving Goldak's ellipsoidal heat source model. For the standard technique the heat source parameters were: $r_x = 3.2$ mm, $r_y = 2.9$ mm, $r_z = 2.8$ mm while for the element birth and death techniques $r_x = 3.4$ mm, $r_y = 2.9$ mm, $r_z = 1.4$ mm. The dwell at the weld start point is set to 1 s. The convective heat transfer (CHT) coefficient is 5.7 W/m^{2}K and radiation emissivity set to 0.75. The heat efficiency is 100%.

INSA-Framatone, France used SYSWELD code with three different moving heat source models: Gaussian surface heat source, conical heat source and prismatic heat source [16]. The heat efficiency was 75%, the CHT coefficient 15 W/m^{2}K and the radiation emissivity 0.7.

The Joint Research Centre, Institute for Energy, Petten, Netherlands [17] used the ANSYS code. The moving heat source was modeled with two different models: melting temperature field and uniform heat generated field. The melting temperature was loaded at prescribed melted zone while at uniform heat generated field uniform heat rate was applied at prescribed melting zone. The heat efficiency was set at 70%. The CHT coefficient was set to 10 W/m^{2}K and no radiation was considered.

Serco, a Technical and Assurance Service, UK [18] used SYSWELD code with Goldak's double ellipsoidal moving heat source model $r_x = 1.6$ mm, $r_y = 3.2$ mm, $r_{z1} = 1.6$ mm and $r_{z2} = 3.2$ mm. The heat efficiency is set to 80% while the overall convective coefficient was 13.57 W/m^{2}K at 100°C.

Three other participants also contributed; these were: The Institute for Nuclear Research—Romania, Korea Power Engineering Company and University of the West of England, UK [13]. The Institute for Nuclear Research used ANSYS code. Uniform heat was generated at nodes inside the melted zone. Convection was modeled with a convective coefficient of 10 W/m^{2}K. The Korea Power Engineering Company used the ABAQUS code with the heat source modeled as a combination of heat flux and body heat load. The heat flux was set to 60% and the body heat load set to 40% of the total heat. The element birth and death technique was used. The CHT coefficient was

Table 3 Properties of materials as a function of temperature [12]

Temperature	Specific heat, c kJ/(kgK)		Conductivity, k W/(mK)	Thermal expansion, α $\times 10^6$ (K^{-1})	Young's modulus (Gpa)	
	Weld	Parent	Weld and parent	Weld and parent	Parent	Weld
20	0.488	0.492	14.12	14.56	195.6	171.0
100	0.502	0.502	15.26	15.39	191.2	165.0
200	0.520	0.514	16.69	16.21	185.7	157.5
300	0.537	0.526	18.11	16.86	179.6	150.0
400	0.555	0.538	19.54	17.37	172.6	142.5
500	0.572	0.550	20.96	17.78	164.5	135.0
600	0.589	0.562	22.38	18.12	155.0	127.5
700	0.589	0.575	23.81	18.43	144.1	120.0
800	0.589	0.587	25.23	18.72	131.4	109.0
900	0.589	0.599	26.66	18.99	116.8	96.9
1,000	0.589	0.611	28.08	19.27	100.0	83.0
1,100	0.589	0.623	29.50	19.53	80.0	66.4
1,200	0.589	0.635	30.93	19.79	57.0	47.3
1,300	0.589	0.647	32.35	20.02	30.0	25.0
1,400	0.589	0.659	33.78	20.21	2.0	1.7

10 W/m^{2}K and the heat efficiency 75%. The University of the West of England also used the ABAQUS code with a uniform moving heat source in the melted zone. The overall convective coefficient at 1,000°C was 89.2 W/m^{2}K while the CHT coefficient was 10 W/m^{2}K and the radiation emissivity 0.4. The heat efficiency was 80%.

From the above, it can be seen that the assumed welding efficiency varied from 60 to 100%. The participants used varied welding efficiency to describe the heat absorbed by the plate. Three participants have used Goldak's heat source model, however the parameters (r_x, r_y and r_z) were different depending on the researcher's assumptions. At the start point of the weld, the participants used varied dwell times, from 0 s (no dwell) up to 1.5 s. The cooling mode due to convection and radiation were modeled using a combination of the following: CHT coefficient, radiation emissivity or overall CHT coefficient; however the values chosen varied widely. In summary it can be seen that the welding models gave different results depending on the basic assumptions made. The current paper presents systematic strategies to produce a validated thermal model of bead-on-plate welding. Based on these strategies it should be possible to arrive at the consistent input parameters for the welding model and correct temperature histories can be provided as well.

4 Welding finite element model

Welding is commonly modeled by moving a heat source over the solid. Three main configurations of moving heat source are used: point heat source, surface heat source and volumetric heat source. In this paper, the volumetric heat source based on the Goldak's ellipsoidal distributed heat source [19] is chosen since it is the most general form of the heat source models. Also from the FEM simulation point of view, the volumetric heat source as a body load has at least two advantages over a surface load: better accuracy and flexibility. The model in this paper is based on a moving heat source over an infinite solid. If the welding process moves parallel to the z axis, and ξ represents a moving abscissa parallel to the z axis, the heat load at a certain small increment volume can be expressed by Eq. 1.

$$\dot{q}'''_{(x,y,\xi)} = \dot{q}'''_0 e^{-Ax^2-By^2-c\xi^2} \tag{1}$$

A, B, C are constants and $\dot{q}'''_0$ is volumetric heat liberated at (0, 0, 0). Considering energy conservation and that welding is applied on a plate, i.e. semi infinite solid, Eq. 2 is obtained.

$$2\dot{q} = 2\eta effVI = 8\int_0^\infty\int_0^\infty\int_0^\infty \dot{q}'''_0 e^{-Ax^2-By^2-C\xi^2}dxdyd\xi \tag{2}$$

It is known mathematically that $\int e^{t^2}dt = \frac{1}{2}\sqrt{\pi}.erf(t)$, and at the limits $\int_0^\infty e^{-t^2}dt = \frac{1}{2}\sqrt{\pi}$. As a result Eq. 2 can be written as in Eq. 3.

$$2\dot{q} = \frac{q'''_0\pi\sqrt{\pi}}{\sqrt{ABC}} \tag{3}$$

For the Gaussian distributed surface disc heat source the heat varies according to distance from the center which is expressed as $\dot{q}'' = Ce^{-3(r_i/r_0)^2}$ [20]. r_i is distance from

center point and r_o is the outside radius of the disc. For $r_i = 0$ the heat flux will have the maximum value of $\dot{q}''_{\max} = C$ whilst for $r_i = r_o$ the minimum heat flux will be $\dot{q}''_{\min} = Ce^{-3}$. Inspite of proposed modifications [21], the ratio between the maximum heat flux at the center of disc and minimum heat flux at the disc center usually is taken as 5%. Similarly, for Goldak heat source model the heat rate that is generated at edge elements is considered equal to 5% of the heat rate applied at the center element. For elements at (r_x, 0, 0), (0, r_y, 0) and (0, 0, r_z) $\dot{q}''_{(x,y,\xi)} = 5\%\dot{q}'''_0$; and using Eqs. 1 and 3, Eq. 4 can be obtained for the Goldak heat source model.

$$\dot{q}'''_{(x,y,\xi)} = \frac{6\sqrt{3}\dot{q}}{\pi\sqrt{\pi}\, r_x r_y r_z} e^{-\frac{3x^2}{r_x^2}} \cdot e^{-\frac{3y^2}{r_y^2}} \cdot e^{-\frac{3\xi^2}{r_z^2}} \tag{4}$$

The maximum value of Eq. 4 is $\dot{q}'''_{\max} = \frac{6\sqrt{3}\dot{q}}{\pi\sqrt{\pi}r_x r_y r_z}$ at position (0, 0, 0). Considering this condition and substituting $r_e^2 = \frac{3x^2}{r_x^2} + \frac{3y^2}{r_y^2} + \frac{3\xi^2}{r_z^2}$, Eq. 4 can be simplified to Eq. 5.

$$\dot{q}'''_{(x,y,\xi)} = \dot{q}'''_{\max} e^{-r_e^2} \tag{5}$$

To obtain a good model of the heat source, a very fine mesh should be provided in the area where the heat source will pass through. Equation 5 can be used to judge how fine the meshes need to be, which depends on r_x, r_y and r_z values; the higher these values the coarser the mesh needs to be. Brick elements of 0.3 mm brick mesh have been used. The adequacy of the mesh size is analyzed after r_x, r_y and r_z values are obtained. Further detailed can be found in Sect. 4.2.

In this paper, finite element model and simulation have been carried out using ANSYS parametric design language (APDL) mode due to its flexibility over the graphics user interface (GUI) mode. A one-half model was used due to symmetry. The model is comprised of 43,639 nodes and 71,128 elements of solid 70 elements. Denser meshes close to the weld line are needed due to high temperature gradient at this position. Very fine meshes in the weld area are needed to match closely the moving heat source. Dense meshes are also applied at positions surrounding a thermocouple to locate thermocouple positions accurately. The final FEM mesh design is shown in Fig. 4.

The general materials properties obtained from https://odin.jrc.ec.europa.eu are given in Table 3 and the thermal properties presented graphically in Fig. 3.

This study used two approaches; a standard approach and an element birth-and-death technique approach. In the standard approach the deposited weld bead is modeled in situ with the welded plate, while in the birth and death techniques the weld deposit metal is developed in accordance with the position of moving heat source model. The standard approach can provide temperature history data faster; although the element birth and death technique are closer to the real condition a longer computer time is needed.

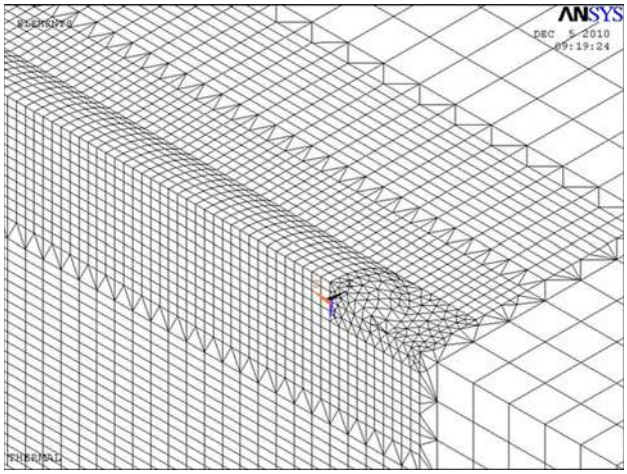

Fig. 4 FEM mesh design

4.1 Solution strategies

Firstly the welding efficiency should be found. Since there are no data provided by NeT, welding efficiency was determined by fitting the peak temperature at Tc9. The thermocouple was chosen since it is least influenced by factors such as heat source model, and heat from arc radiation. Only global heat input affects it significantly. Moreover the thermocouple indicates the temperature at the quasi steady state and it is easy to locate accurately in FEM mesh. Normally the welding efficiency of TIG ranges between 65 and 88% [22]. A preliminary estimation of the welding efficiency was made based on a simple model. This preliminary welding efficiency is needed to avoid large number of trial and error in the final model. The welding model is

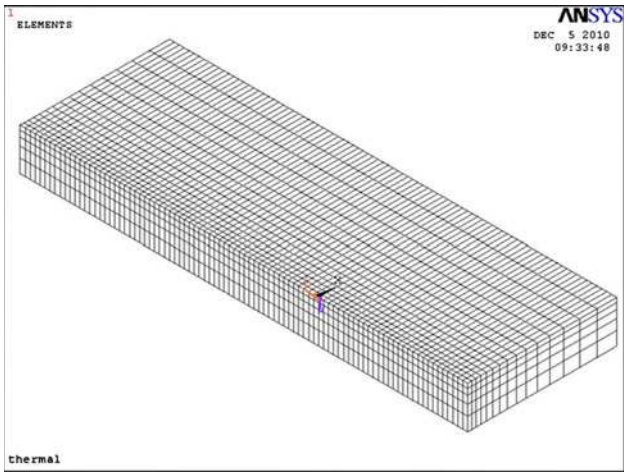

Fig. 5 Simplified FEM mesh design

made simple using a moving point heat source to save computer time. The finite element mesh of the simplified model is shown at Fig. 5. A stepped mesh was used to decrease the number of elements. The heat rate intensity $\dot{q}$ (J/s) can be calculated from the product of the heat input time and welding speed. Data of the heat input and welding speed are obtained from NeT. Observing peak temperature at Tc9 of the simulation result on simplified model, the preliminary welding efficiency was found to be 76%.

The second step is the modeling of moving heat source on the final model. Using Goldak's ellipsoidal heat source as expressed in Eq. 4. The value of $\dot{q}$ can be obtained from the product of heat input (633 J/mm) and welding speed (2.27 mm/s). Other parameters (r_x, r_y, r_z) were tentatively determined by fitting mid length thermocouples peak temperature (Tc2, Tc5 and Tc7). It should be noted that, the APDL code can accommodate adjustable r_x, r_y and r_z. The mid-length thermocouples are insensitive to arc dwell and initiation mode at weld start point, also insensitive to the arc extinction model at the weld end point. At this stage, definitive welding efficiency can be determined by fitting peak temperature at the bottom face thermocouple (Tc9) and mid length thermocouples (Tc2, Tc5 and Tc7).

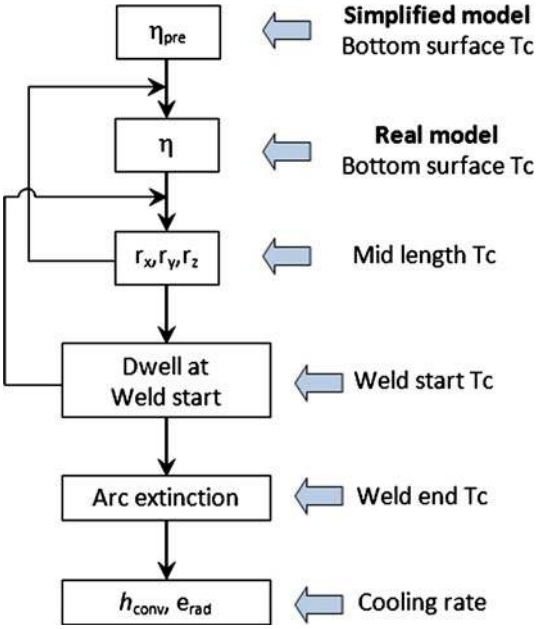

Fig. 6 Steps to provide validated thermal analysis

The third step is the modeling of the arc dwell and initiation at the weld start point. The arc dwelling time is modeled mainly by fitting peak temperature of thermocouples at the start end (Tc1, Tc4). Two choices of arc initiation mode can be used, either a stepped load mode or a ramped load mode. Meanwhile, the tentative heat source parameters can be altered to fit peak temperature at the start end (Tc1, Tc4) and mid length (Tc2, Tc5 and Tc7).

The fourth step is the modeling of arc extinction at the weld end point. An evaluation is made of the thermocouples at the weld end for close field and far field, Tc3 and Tc6 respectively. The arc extinction was modeled by a ramp load which is removed after 0.001 s.

The modeling of convection and radiation at the welded plate surfaces is the final step. The parameters for convection (h_{conv}) and radiation (e_{rad}) were determined so as to match the cooling rate determined at all thermocouples. Using this procedure, it was found that the convection heat transfer coefficient is 5 (watt/m^2 K) and emissivity is 0.5. The steps taken to determine the temperatures history are shown as flowchart in Fig. 6.

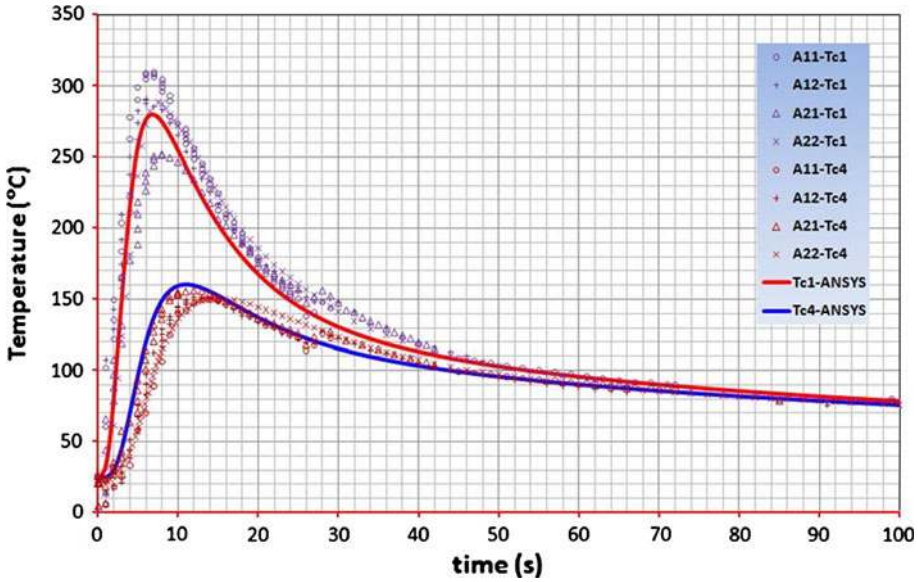

Fig. 7 Temperature histories using standard technique for location of thermocouple Tc1 & Tc4 (refer to Fig. 2)

4.2 Standard technique

In the standard technique the weld metal bead is modeled before the moving heat source load is simulated. The moving heat source is modeled by applying the Goldak's ellipsoidal model at a certain point and heat is liberated for a given time duration depending on the welding speed and distance between a point with the next consecutive point. The distance is determined by the mesh size of the FEM model. Since the mesh size on the heat source path is 0.3 mm and the welding speed is 2.27 mm/s, the time duration is 0.1322 s, after which the heat source is removed and is relocated to the next position and liberates heat for the same time duration. This procedure is repeated until the end of the weld length.

Following the NeT procedures, it should be noted that the data are obtained from four tests (A11, A12, A21 and A22) and each test is comprised of nine initial temperature data (Tc1–Tc9). The initial temperatures varied between 21°C up to 29°C. From the NeT temperature histories, the initial temperature of the base metal was assigned as 25°C. This initial temperature was the mean value of initial temperatures shown by the thermocouple data. Fitting peak temperatures of "real" model at Tc9, the preliminary welding efficiency was calculated to be 80%. The heat source parameters $r_x = 5$ mm, $r_y = 2$ mm, $r_z = 3$ mm (Eq. 4) were obtained after evaluating peak temperatures at the mid length position. The dwell time at the weld start is 1 s which is obtained after evaluating the peak temperature at weld start thermocouples (Tc1, Tc4).

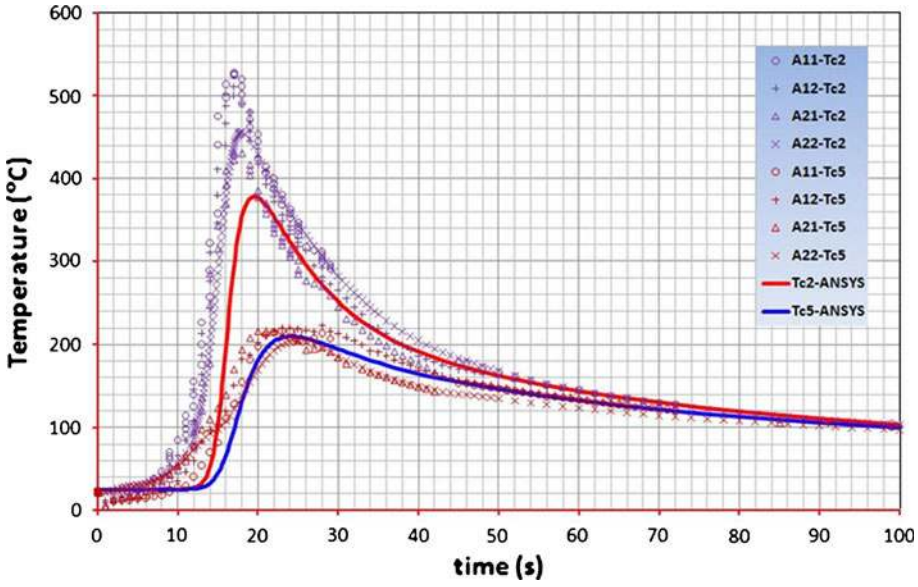

Fig. 8 Temperature histories using standard technique for location of thermocouple Tc2 & Tc5 (refer to Fig. 2)

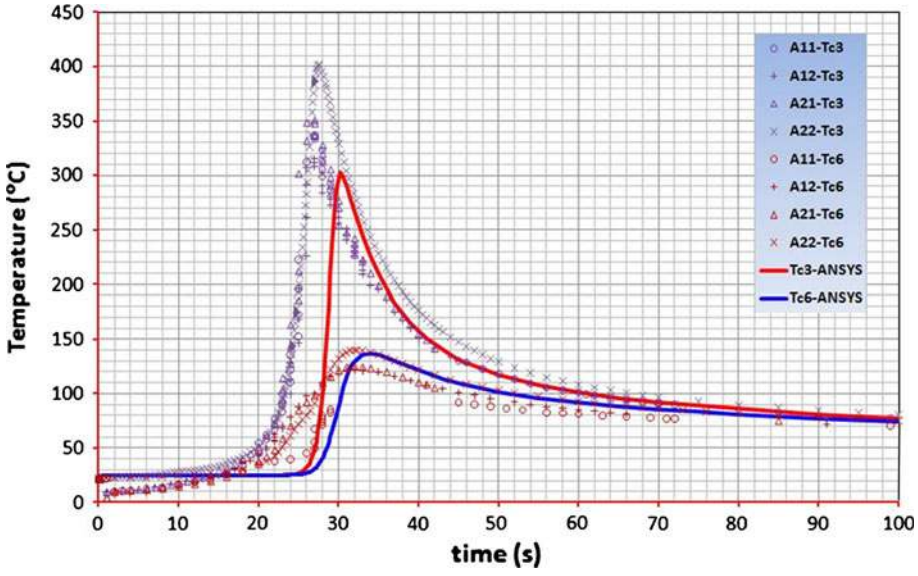

Fig. 9 Temperature histories using standard technique for location of thermocouple Tc3 & Tc6 (refer to Fig. 2)

Brick mesh sizes along the heat source trajectory are 0.3 mm. The body heat source values depend on the distance from the centroid of the elements to the center of the heat source. Since the brick mesh sizes are 0.3 mm, the closest r_e^2 is 0.02708 mm^2 which when applied to Eq. 5 results in $\dot{q}'''_{(x,y,\xi)} = 0.9733 q'''_{\max}$. The maximum body heat will be represented by 97.33% of its value, and it can be assumed that the mesh size along the weld path is sufficiently fine.

4.3 Birth and death technique

In the element birth and death technique, the metal bead is growing with the moving heat source. First, all of weld bead elements are "omitted" using EKILL command in ANSYS and the growth is modeled using EALIVE command. Born elements are elements of the weld bead which are already left behind the moving heat source. When the elements are born, their temperature should be at the melting embedded filler metal temperature which is superheated at 2,400°C [23]. Instead of applying temperature node load, the body heat load rate $(\dot{q}''')$ at elements was applied. The body heat load value is such that it can produce a temperature of 2,400°C at the growing weld bead. The heat needed to elevated the weld pool from the initial temperature of 25–2,400°C was evaluated using $q = mc\Delta T$. It should be noted that the specific heat c, is temperature-dependent as expressed in Table 3. The specific heat at a certain

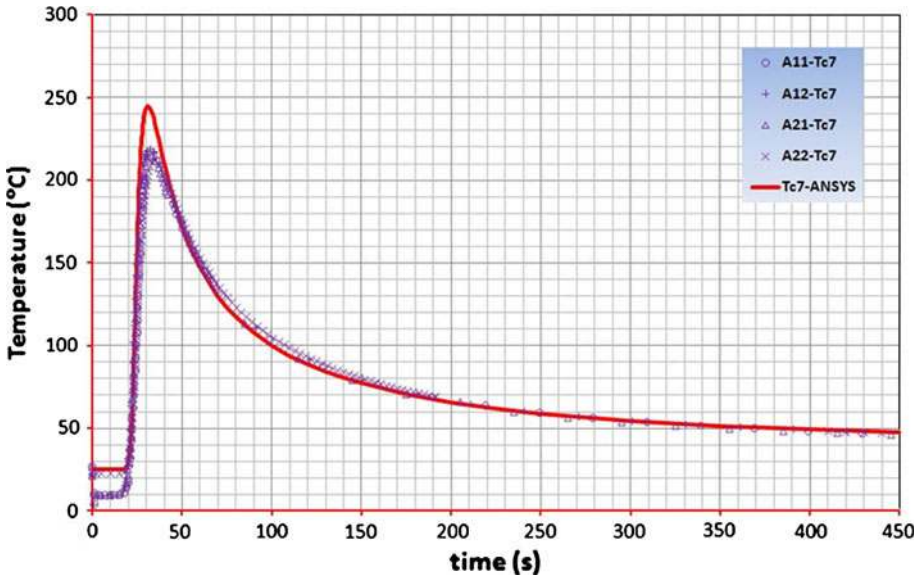

Fig. 10 Temperature history using standard technique for location of thermocouple Tc7 (refer to Fig. 2)

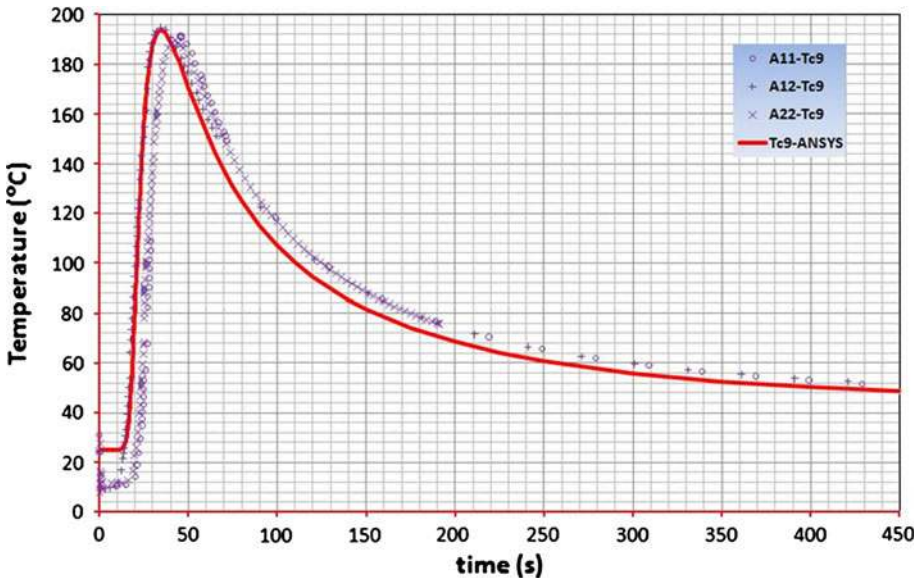

Fig. 11 Temperature history using standard technique for location of thermocouple Tc9 (refer to Fig. 2)

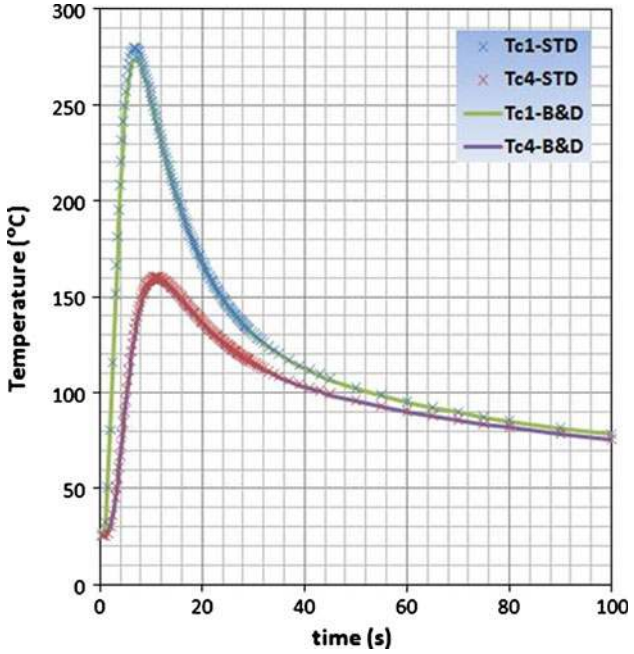

Fig. 12 Temperature histories using standard and birth & death techniques for location of thermocouple Tc1 & Tc4 (refer to Fig. 2)

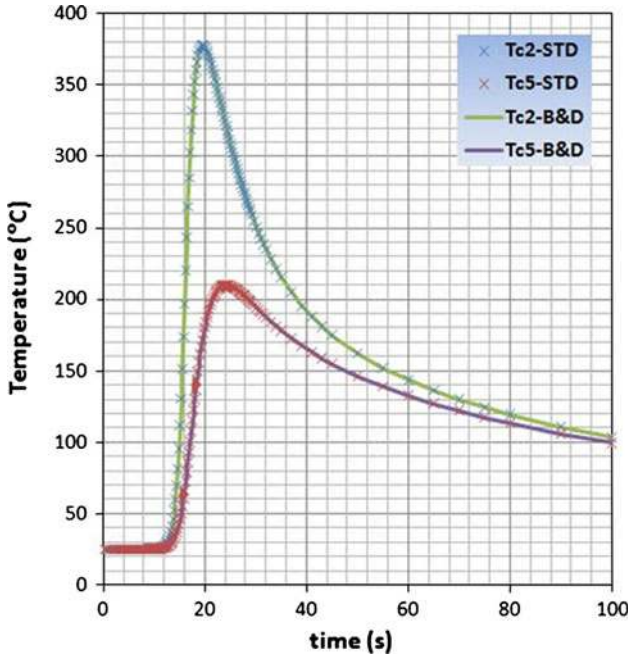

Fig. 13 Temperature histories using standard and birth & death techniques for location of thermocouple Tc2 & Tc5 (refer to Fig. 2)

temperature range was taken as the mean value between these ranges. The heat rate can be obtain using $\dot{q} = mc\Delta T\left(\frac{S}{v}\right)$expression. Finally, the body heat load which should be applied at the born weld bead can be obtained using Eq. 6.

$$\dot{q}''' = \rho c \Delta T \left(\frac{S}{v}\right) \tag{6}$$

5 Results and discussion

The temperature histories for the standard technique are shown in Figs. 7, 8, 9, 10, 11. To fit peak temperature especially at Tc9, $\eta_{\text{weld}} = 80\%$ was used. It should be noted that this value lies within the theoretical ranges. From these figures it can be claimed that this simulation has shown a good agreement with experimental results. Apart from showing the general trend, the transient temperature values also match the experimental data. For the close field thermocouples, especially at mid length and the weld end (Tc2 and Tc3) the FEM model predicts a lower temperature than the measured peak temperature. The lower prediction may be caused by the radiation of torch arc which was not modeled. The 'below bead' thermocouple (Tc7), the model shows a higher value than that measured by the thermocouple. The 'below bead' thermocouple was inserted 6.5 mm deep in a hole with diameter of 1.2 mm. The possibility that the thermocouple is not fully located at the tip of the hole is high. Incomplete insertion could result in a larger distance from the heat source and a lower measured peak temperature. If the measured point is only 0.5 mm further from the heat source, an evaluation using the ANSYS model showed that

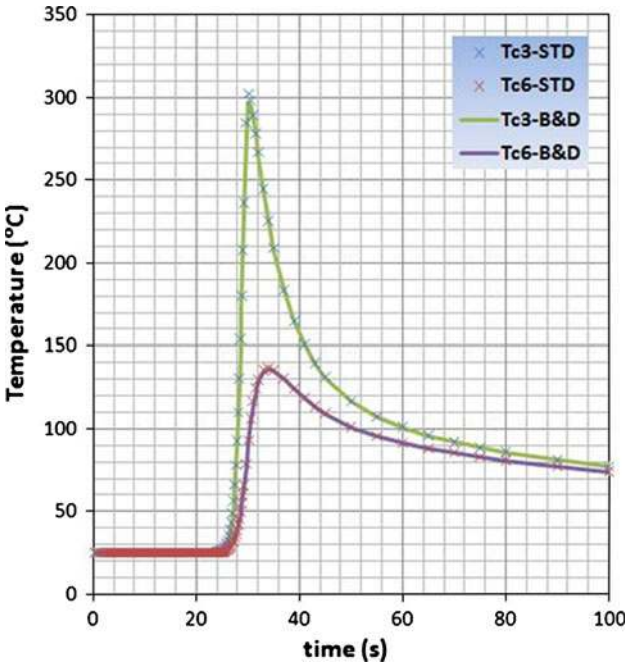

Fig. 14 Temperature histories using standard and birth & death techniques for location of thermocouple Tc3 & Tc6 (refer to Fig. 2)

the peak temperature will fit with the measured peak temperature.

Using the birth and death technique, a weld efficiency $\eta_{\text{weld}} = 73\%$ is required to fit peak temperatures especially at Tc9. It should be noted that this is lower than weld efficiency which is obtained using standard technique (80%). The higher weld efficiency of the standard technique means that the higher heat input is required to heat weld bead which is actually not existed before the filler metal is dropped there, or in term of the element birth and death techniques before it is born. Another reason for the higher heat input in standard technique is the ignorance on heat which is generated by the high temperature of weld bead. The predicted temperature histories at the thermocouple positions resulting from the application of both techniques are shown in Figs. 12, 13, 14, 15. It can be seen that temperature profiles using both techniques are in good agreement.

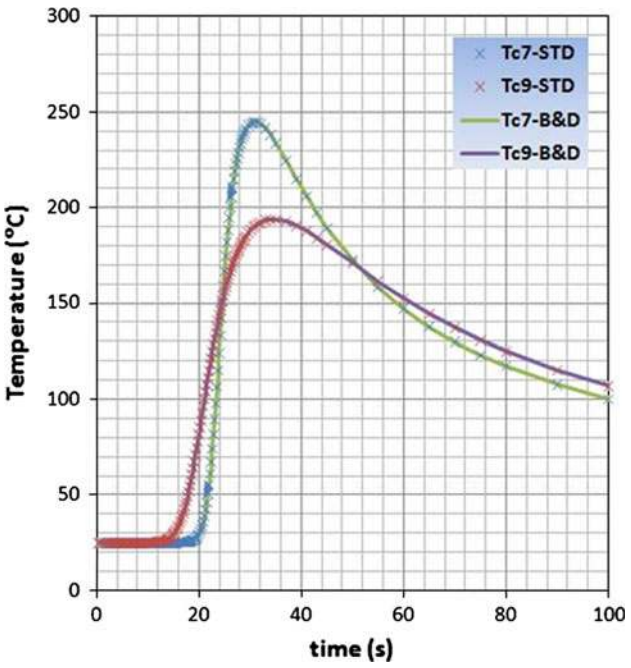

Fig. 15 Temperature histories using standard and birth & death techniques for location of thermocouple Tc7 & Tc9 (refer to Fig. 2)

5.1 Weld pool shape

Weld pool shape at the mid length cross section is compared with actual weld pool shape in Figs. 16 and 17 for both techniques. The actual weld pool cross section is obtained by cutting the welded plate. The weld pool shape predicted by the FEM model is the region where the temperature is above 1,400°C (melting point of AISI 316 stainless steel). It can be seen that the weld pool can be modeled well using both techniques which follow the procedure shown in Fig. 6. In Fig. 18 the weld pool sections predicted by both techniques is compared. Although the temperature distribution especially for high temperature above 1,900°C shows different distribution for both techniques, the weld pool shape is same. The high temperature at the weld bead center in the birth and death technique occupied a larger area (red area) which is caused by the existence of higher droplet temperature.

6 Conclusion

A comprehensive model of transient thermal behavior of a weld has been established and validated using experiment

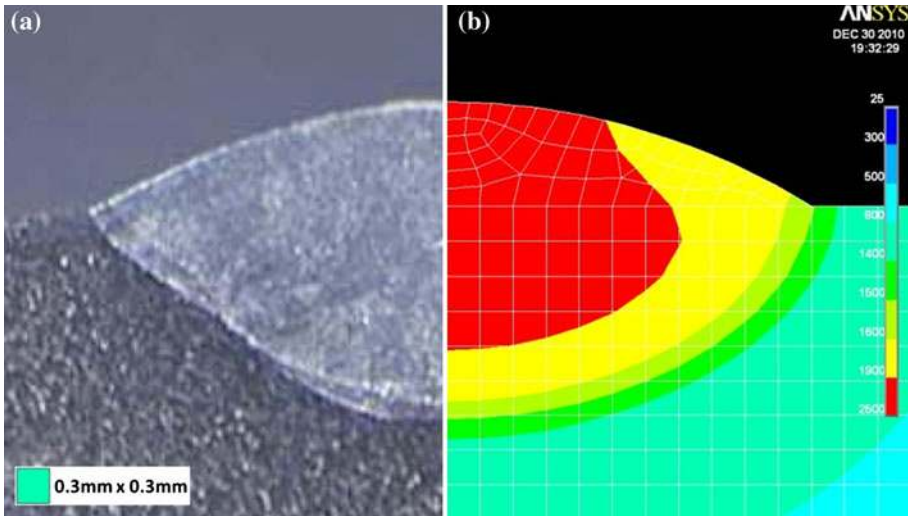

Fig. 16 **a** Weld pool of actual weld and **b** temperature contour from standard technique

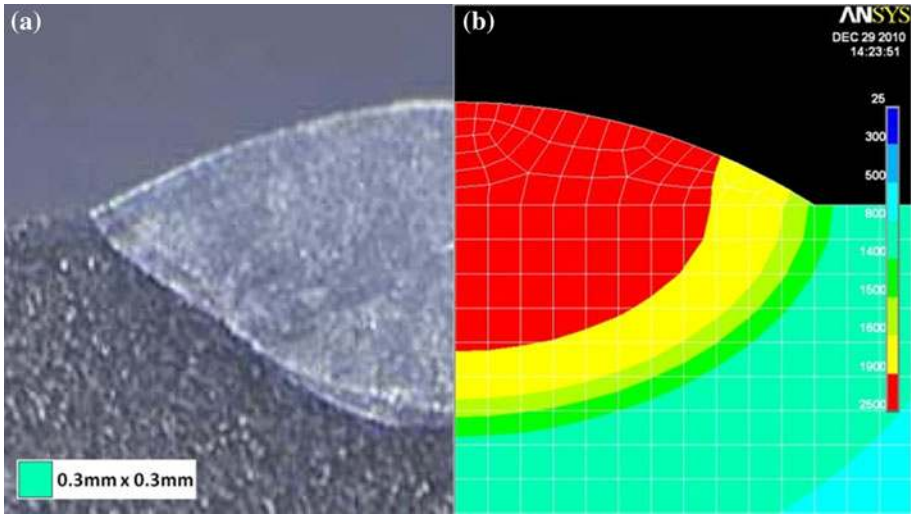

Fig. 17 **a** Weld pool of actual weld and **b** temperature contour from birth to death technique

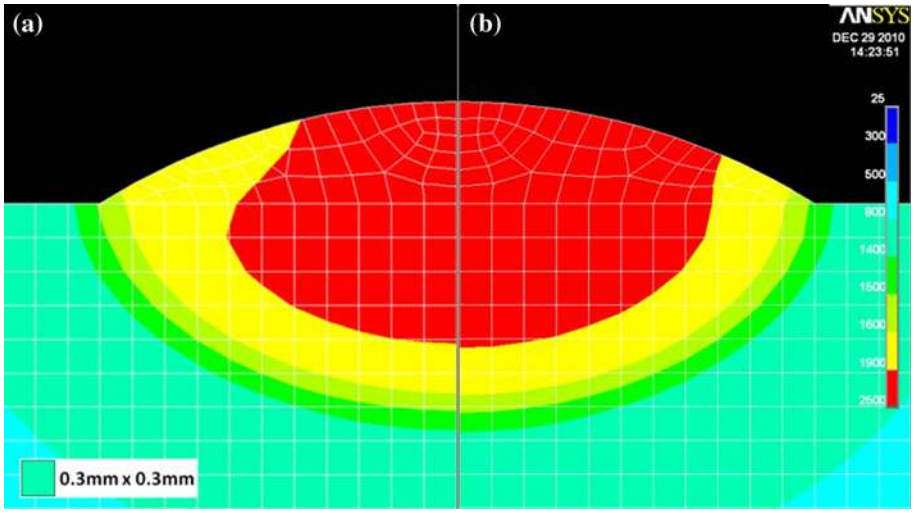

Fig. 18 Comparison of temperature contour. **a** Standard technique, **b** birth and death technique

results from the NeT consortium. The proposed approach can provide a consistent and good match temperature history with the measured data. The methodology proposed here can provide validated thermal analysis using both standard and birth-and-death techniques.

The higher heat input needed in the standard techniques is caused by two reasons: neglecting high temperature of melting filler metals and a part of heat that should be transferred to the weld bead which is actually not existed.

Predicted weld pool shape using standard technique and birth-and-death technique show well match results. The evaluation of predicted weld pool shape enhances the validity of the welding model.

References

1. Xu J, Chen L, Ni C (2007) Effect of vibratory weld conditioning on the residual stresses and distortion in multi-pass girth-butt welded pipes. Press Vessel Pip 84:298–303
2. Murugananth M, Bhadeshia HKDH, Keehan E, Andren HO, Karlson L (2002) Mathematical modelling of weld phenomena—6. In: Strong and tough steel welds. Institute of Material, Graz University of Technology, pp 205–229
3. Keehan E, Andrea HO, Karlsson L, Murugananth M, Bhadeshia HKPH (2002) Mechanical effects of nickel and manganese on high strength steel weld metal. Recent Trends in Welding Research, Atlanta
4. Ilman MN, Triyono (2010) Fatigue crack growth behaviour of friction stir welded aluminium alloy 2024-T3 under local pre-heating. Int J Mater Sci 5(6):791–800

5. Deaconu V (2007) Finite element modeling of residual stress—a powerful tool in the aid of structural integrity assessment of welded structures. 5th International Conference Structural Integrity of Welded Structures, Romania
6. Rosenthal D (1946) The theory of moving source of heat and its application to metal transfer. Trans ASME 43(11):849–866
7. Carslaw HS, Jaeger JC (1959) Conduction of heat in solid. Clarendon Press, Oxford
8. Paley ZVI, Lynch JN, Adam CM Jr (1964) Heat flow in welding heavy steel plate. Welding Research Supplement, pp 71–79
9. Christensen N, Davies V, Gjermundsen K (1965) Distribution of temperature in arc welding. Br Weld J 12(2):54–75
10. Tsai CL (1982) Heat flow in fusion welding. In: Proceeding of the conference on trends in welding research in the United States. ASM International, New Orleans, pp 91–108
11. Truman CE, Smith MC (2009) The NeT residual stress measurement and modeling round robin on a single weld bead-on-plate specimen. Int J Press Vessel Pip 84:1–2
12. Protocol for phase 2 finite element simulation on the NET single-bead-on-plate test specimen. https://odin.jrc.ec.europa.eu
13. Smith MC, Smith AC (2009) NeT bead-on-plate round robin: comparison of transient thermal prediction and measurements. Int J Press Vessel Pip 86:96–109
14. Ficquet X, Smith DJ, Truman CE, Kingston EJ, Dennis RJ (2009) Measurement and prediction of residual stress in a bead-on-plate weld benchmark specimen. Int J Press Vessel Pip 86:20–30
15. Shan X, Davies CM, Wangsdan T, O'Dowd NP, Nikbin KM (2009) Thermo-mechanical modeling of a single-bead-on-plate weld using the finite element method. Int J Press Vessel Pip 86:110–121
16. Gilles P, El-Ahmar W, Jullien J-F (2009) Robustness analyses of numerical simulation of fusion welding NeT-TG1 application: "single weld-bead-on-plate". Int J Press Vessel Pip 86:3–12
17. Ohms C, Wimpory RC, Katsareas DE, Youtsos AG (2009) NeT TG1: residual stress assessment by neutron diffraction and finite element modeling on a single bead weld on a steel plate. Int J Press Vessel Pip 86:63–72
18. Bate SK, Charles R, Warren A (2009) Finite element analysis of a single bead-on-plate specimen using SYSWELD. Int J Press Vessel Pip 86:73–78
19. Goldak J, Chakravarti A, Bibby M (1982) A new finite element model for welding heat sources. Metall Trans B 15B:299–305
20. Komanduri R, Hou ZB (2000) Thermal analysis of the arc welding process: part i. general solutions. Metall Mater Trans B 31B:1353–1370
21. Roshyana NR (2009) Correct modeling for gaussian distributed heat source on a finite thin rod. Heat Mass Transf 45:1253–1260. doi:10.1007/s00231-009-0498-5
22. Kou S (2003) Welding metallurgy. Wiley, London
23. Painter MJ, Davies MH (1994) Numerical modeling of the gas metal arc welding process. Annual Report—CRC Project: 93.04